

# Behaviour of the Serre Equations in the Presence of Steep Gradients Revisited

Jordan Pitt,<sup>1</sup>  
Christopher Zoppou,<sup>1</sup>  
Stephen G. Roberts,<sup>1</sup>

## ABSTRACT

**Keywords:** dispersive waves, conservation laws, Serre equation, finite volume method, finite difference method

## 1 INTRODUCTION

2 The behaviour of steep gradients in a flow is important to shallow water modelling  
3 both because there are problems in which steep gradients are present in the initial  
4 conditions such as the propagation of a bore or the classical dam-break problem and  
5 also because some problems develop steep gradients as they evolve such as shoaling  
6 waves on a beach.

7 For our shallow water model of interest the Serre equations there are no analytic  
8 solutions to problems containing steep gradients. Although expressions have been  
9 derived for some important quantities such as the leading wave height and speed of an  
10 undular bore (El et al. 2006). Therefore to understand the more general structure of  
11 solutions to problems containing steep gradients we must turn to numerical methods  
12 to give us some insight.

13 Unfortunately there are few results which depict the behaviour of numerical solu-  
14 tions to the Serre equations in the presence of steep gradients (El et al. 2006; Le Métayer  
15 et al. 2010; Mitsotakis et al. 2016; Mitsotakis et al. 2014). These papers all present  
16 either travelling bores or the dam break problem and for two they present the same  
17 dam-break problem at different times (El et al. 2006; Le Métayer et al. 2010). There  
18 is however disagreement about the true nature of the solutions to these problems based  
19 on the presented numerical results.

20 Most of these papers have used some smoothing of the initial conditions to approx-  
21 imate the steep gradients present in the problem (El et al. 2006; Mitsotakis et al. 2016;

---

<sup>1</sup>Mathematical Sciences Institute, Australian National University, Canberra, ACT 0200, Australia,  
E-mail: Jordan.Pitt@anu.edu.au. The work undertaken by the first author was supported financially by  
an Australian National University Scholarship.

22 Mitsotakis et al. 2014). There have also been comparisons for the dam-break problem  
 23 between the analytic solutions of the shallow water wave equations and in some sense  
 24 the mean behaviour of numerical results for the Serre equations (Le Métayer et al.  
 25 2010; Mitsotakis et al. 2014).

26 This paper makes use of a first, second and third-order numerical method (Zoppou  
 27 et al. 2017) that is robust to steep gradients, with the first-order method being a recre-  
 28 etion of the numerical method of Le Métayer et al. (2010). This paper also make use of  
 29 two finite difference schemes, one is a recreation of the method of El et al. (2006) and  
 30 the other is a naive finite difference approximation that makes for a good comparison.

31 These five different methods were then all used on the common dam-break problem  
 32 (El et al. 2006; Le Métayer et al. 2010) to explain the disagreements in the nature of  
 33 the solutions. It was found that the results of Le Métayer et al. (2010) were restricted  
 34 by the diffusivity of the numerical method. While the results for the other papers were  
 35 impacted by the smoothing of the initial conditions (El et al. 2006; Le Métayer et al.  
 36 2010). Through this process a new behaviour for our numerical results was found  
 37 which has hitherto not been depicted. We also found that the analytic solutions for the  
 38 shallow water wave equations are not precisely the mean behaviour of our solutions  
 39 and our solutions disagree slightly with the Whitham modulation results of El et al.  
 40 (2006).

41 The paper is organised as follows: The Serre equations are given as well as some  
 42 important properties for validation, a reproducible expression of the two finite differ-  
 43 ence methods are given as well as the reformulation of the Serre equations into conser-  
 44 vative form. Some numerical results are presented for the soliton problem to validate  
 45 the finite difference methods and then the results of our numerical investigation into  
 46 the behaviour of the Serre equations applied to the dam-break problem are presented.

## 47 SERRE EQUATIONS

48 The Serre equations can derived by integrating the full incompressible Euler equa-  
 49 tions over the water depth, see for example Su and Gardner (1969). They can also be  
 50 derived as an asymptotic expansion of the Euler equations, see for example Lannes and  
 51 Bonneton (2009). Assuming a constant horizontal bed the Serre equations are (Li et al.  
 52 2014)

$$53 \quad \frac{\partial h}{\partial t} + \frac{\partial(uh)}{\partial x} = 0 \quad (1a)$$

54 and

$$56 \quad \underbrace{\frac{\partial(uh)}{\partial t} + \frac{\partial}{\partial x} \left( u^2 h + \frac{gh^2}{2} \right)}_{\text{Shallow Water Wave Equations}} + \underbrace{\frac{\partial}{\partial x} \left( \frac{h^3}{3} \left[ \frac{\partial u}{\partial x} \frac{\partial u}{\partial x} - u \frac{\partial^2 u}{\partial x^2} - \frac{\partial^2 u}{\partial x \partial t} \right] \right)}_{\text{Dispersion Terms}} = 0. \quad (1b)$$

57 Where  $u$  is the average horizontal velocity over the depth of water  $h$ ,  $g$  is the accelera-  
 58 tion due to gravity,  $x$  is the horizontal spatial variable and  $t$  is time.

60 **Conservation Laws**

61 The Serre equations conserve mass ( $h$ ), momentum ( $uh$ ) and the Hamiltonian ( $\mathcal{H}$ )  
 62 (Li 2002; Green and Naghdi 1976), thus our numerical methods should reflect this.  
 63 The total amount of a quantity  $q$  in a system occurring on the interval  $[a, b]$  is measured  
 64 by

65 
$$\mathcal{C}_q(t) = \int_a^b q(x, t) dx.$$
  
 66

67 Conservation implies that  $\mathcal{C}_h(0) = \mathcal{C}_h(t)$ ,  $\mathcal{C}_{uh}(0) = \mathcal{C}_{uh}(t)$  and  $\mathcal{C}_{\mathcal{H}}(0) = \mathcal{C}_{\mathcal{H}}(t) \forall t$   
 68 provided the interval is fixed and the system is closed.

69 The Hamiltonian is

70 
$$\mathcal{H}(x, t) = \frac{1}{2} \left( hu^2 + \frac{h^3}{3} \left( \frac{\partial u}{\partial x} \right)^2 + gh^2 \right) \quad (2)$$
  
 71

72 representing the energy in the system and is the sum of the kinetic energies in the hor-  
 73 izontal ( $hu^2$ ) and vertical ( $\frac{h^3}{3} \left( \frac{\partial u}{\partial x} \right)^2$ ) directions and the gravitational potential energy  
 74 ( $gh^2$ ).

75 **SMOOTHED DAM-BREAK**

76 The discontinuous dam-break problem can be approximated smoothly using the  
 77 hyperbolic tangent function. Such an approximation will be called a smoothed dam-  
 78 break problem and will be defined as such

79 
$$h(x, 0) = h_0 + \frac{h_1 - h_0}{2} \left( 1 + \tanh \left( \frac{x_0 - x}{\alpha} \right) \right), \quad (3a)$$
  
 80

81

82 
$$u(x, 0) = 0.0m/s. \quad (3b)$$
  
 83

84 Where  $\alpha$  measures the distance over which 46.117% of the smooth transition between  
 85 the two heights of  $h_0$  and  $h_1$  centered around  $x_0$  occurs. Figure 1 demonstrates the  
 86 effect of varying  $\alpha$  for the smoothed dam-break problem with  $h_1 = 1.8m$ ,  $h_0 = 1m$   
 87 and  $x_0 = 500m$ . These are the same  $h_0$  and  $h_1$  values as those of the dam-breaks  
 88 presented by El et al. (2006) and Le Métayer et al. (2010) and will be the values used  
 89 throughout this paper.

90 From (3) the following expressions for  $\mathcal{C}_h(0)$ ,  $\mathcal{C}_{uh}(0)$  and  $\mathcal{C}_{\mathcal{H}}(0)$  were derived  
 91 provided  $x_0$  is the midpoint of the spatial domain  $[a, b]$  in which the smoothed dam-  
 92 break occurs

93 
$$\mathcal{C}_h(0) = \frac{h_1 + h_0}{2} (b - a),$$
  
 94

95

96 
$$\mathcal{C}_{uh}(0) = 0$$
  
 97

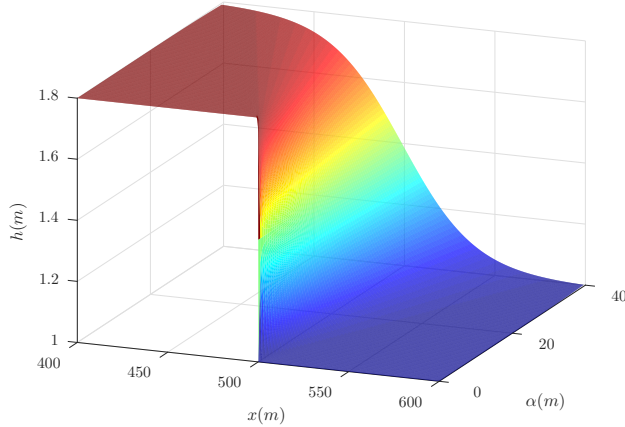


FIG. 1: Initial conditions for the smooth dam-break problem with  $h_0 = 1m$ ,  $h_1 = 1.8m$  and  $x_0 = 500m$  as  $\alpha$  varies.

98 and

$$99 \quad 100 \quad \mathcal{C}_H(0) = \frac{g}{4} \left( h_0^2 - h_1^2 + \alpha (h_1 - h_0)^2 \tanh \left( \frac{a - b}{2\alpha} \right) \right).$$

101 Note that due to a difference in heights at the two boundaries there is a flux of  
102 momentum into the system equal to  $t g(h^2(b) - h^2(a))$  and this must be accounted for in  
103  $C_1$  of  $uh$ .

104 The dam-break problem for the Serre equations results in the creation of an undular  
105 bore that is very similar to the analytic solution of the dam-break problem for the  
106 shallow water wave equations with oscillations (Le Métayer et al. 2010; Mitsotakis  
107 et al. 2014). Because the analytic solution to the dam-break problem for the shallow  
108 water wave equations will be used as a reference in this paper we present it in Figure  
109 2 for  $h_0 = 1m$ ,  $h_1 = 1.8m$  and  $x_0 = 500m$  at  $t = 30s$ . The regions I through V  
110 in Figure 2 will be used to simplify our explanations later on for numerical solutions  
111 of the Serre equations. We also present equations for the quantities of interest in the  
112 analytic solution of the dam-break problem for the shallow water wave equations; the  
113 constant height ( $h_2$ ) and velocity ( $u_2$ ) in regions III and IV and the speed of the shock  
114 ( $S_2$ ) which marks the boundary between regions IV and V. From Wu et al. (1999) we  
115 have the following equations

$$116 \quad 117 \quad 118 \quad h_2 = \frac{h_0}{2} \left[ \sqrt{1 + 8 \left( \frac{2h_2}{h_2 - h_0} \frac{\sqrt{gh_1} - \sqrt{gh_2}}{\sqrt{gh_0}} \right)^2} - 1 \right], \quad (5a)$$

$$119 \quad 120 \quad u_2 = 2 \left( \sqrt{gh_1} - \sqrt{gh_2} \right) \quad (5b)$$

121 and

$$122 \quad 123 \quad S_2 = \frac{h_2 u_2}{h_2 - h_0}. \quad (5c)$$

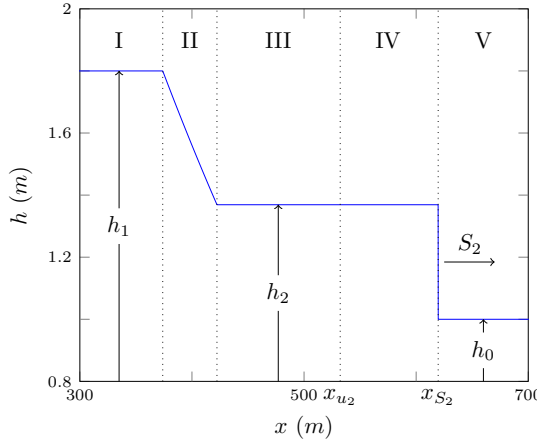


FIG. 2: Analytic solution at  $t = 30s$  of the shallow water wave equations for the dam-break problem with  $h_0 = 1m$ ,  $h_1 = 1.8m$  and  $x_0 = 100m$ .

From these values we also define  $x_{u_2}(t) = x_0 + u_2 t$  and  $x_{S_2}(t) = x_0 + S_2 t$  to give the location of a fluid particle starting at  $x_0$  travelling at speed  $u_2$  and  $S_2$  respectively at time  $t$ .

Undular bores for the one dimensional Serre equations were analysed by El et al. (2006) and an expression for the amplitude ( $A^+$ ) and speed ( $S^+$ ) of the leading wave of a bore shown in Figure 3 were given

$$\frac{\Delta}{(A^+ + 1)^{1/4}} - \left( \frac{3}{4 - \sqrt{A^+ + 1}} \right)^{21/10} \left( \frac{2}{1 + \sqrt{A^+ + 1}} \right)^{2/5} = 0 \quad (6a)$$

$$S^+ = \sqrt{g(A^+ + 1)} \quad (6b)$$

where  $\Delta = h_b/h_0$ , and  $h_b$  is the amplitude of the bore. From this we define  $x_{S^+}(t) = x_0 + S^+ t$  which is the location of a fluid particle starting at  $x_0$  and travelling at speed  $S^+$  at time  $t$ .

The simulations were run with various values of  $\Delta x$  and  $\alpha$ . In regions III and IV there is a background flow and so  $\mathcal{E}$  is unstable, to account for this the growth factor was suppressed by using a smaller time step than the CFL condition of  $\Delta t = 0.01\Delta x$ .  $\mathcal{V}_2$  requires an input parameter to its slope limiter and this was chosen to be  $\theta = 1.2$  (Zoppou et al. 2017). The first set of scenarios presented were run until  $t = 30s$  on the interval  $x \in [0m, 1000m]$ .

Applying (5) to our dam-break problem results in  $h_2 = 1.36898m$ ,  $u_2 = 1.074975 m/s$  and  $S_2 = 3.98835 m/s$  which can be seen in Figure 2. For (6) as in El et al. (2006) the height of the bore is given as

$$h_b = \frac{\left( \sqrt{\frac{h_1}{h_0}} + 1 \right)^2}{4}.$$

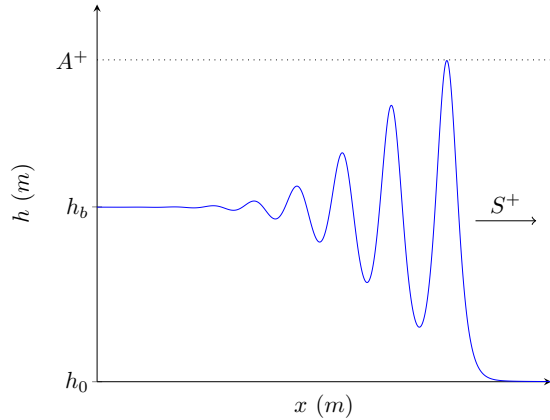


FIG. 3: Demonstration of quantities obtained by Whitham modulation for undular bores of the Serre equations.

143 Thus  $h_b = 1.37082 \text{ m}$ ,  $\Delta = 1.37082$ ,  $A^+ = 1.73998 \text{ m}$  and  $S^+ = 4.13148 \text{ m/s}$ .  
 144 Note that due to the different natures of bores for the Serre and shallow water wave  
 145 equations  $S^+ \neq S_2$ .

## 146 Results

147 We begin this study by looking into the effect of the initial steepness of the smoothed  
 148 dam-break problem for different  $\alpha$  values by observing what happens as  $\Delta x \rightarrow 0$  and  
 149 our numerical solution better approximates the true solution of the Serre equations. To  
 150 have the smallest error we use the highest order well validated model  $\mathcal{V}_3$  in the fol-  
 151 lowing investigation. From these results we then investigate numerical results for long  
 152 time scales, how the shallow water wave equations analytic solution and El's Whitham  
 153 modulation values compare to our results and then finally present some other findings  
 154 about the behaviour of our numerical solutions.

### 155 Effect of $\alpha$

156 Because the smoothing process is a non-physical numerical tool we first study its  
 157 effect by decreasing  $\alpha$  and thus better approximating the dam-break. To do this we fix  
 158 an  $\alpha$  and then investigate the numerical solutions as  $\Delta x \rightarrow 0$  and our well validated  
 159 numerical method better approximates the true solution of the Serre equations.

160 The first observation is that there are four types of behaviour as  $\Delta x \rightarrow 0$  depending  
 161 on the  $\alpha$  and the numerical method. The four behaviours are identified by the nature  
 162 of the solutions around  $x_{u_2}$  when  $\Delta x$  is small and they correspond to different results  
 163 presented in the literature. For brevity the only given examples of these behaviours will  
 164 be the solutions of  $\mathcal{V}_3$  although they all also occurred for the  $\mathcal{E}$ ,  $\mathcal{G}$  and  $\mathcal{V}_2$  simulations  
 165 using the same  $\alpha$  and  $\Delta x = 10/2^{10} \text{ m}$ .

166 The first behaviour which will be referred to as the non-oscillatory behaviour has  
 167 such smooth initial conditions that no oscillations were introduced by  $t = 30\text{s}$  for  
 168 the numerical simulations, although given sufficient time the front steepens and an  
 169 undular bore will develop. This behaviour is not present in the literature as no authors  
 170 chose large enough  $\alpha$  values. An example of this behaviour can be seen in Figure 4

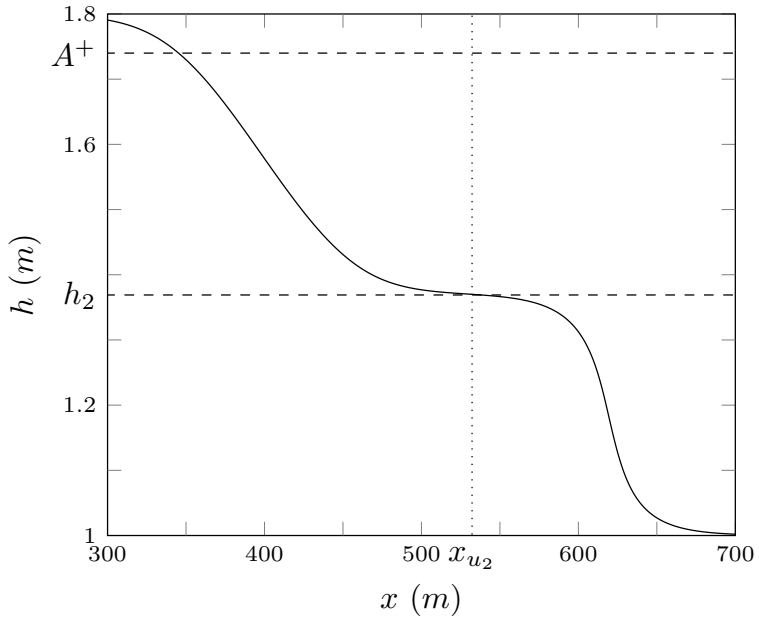


FIG. 4: Numerical results of  $\mathcal{V}_3$  at  $t = 30s$  for the smooth dam-break problem with  $\alpha = 40m$  for  $\Delta x = 10/2^4 m$  (—).

for  $\alpha = 40m$ . Because this is a very smooth problem we observe that all numerical results are visually identical for all  $\Delta x < 10/2^4 m$ . We observed this behaviour for  $\mathcal{V}_1$ 's simulations as well. We note that  $\mathcal{V}_3$ 's numerical solution has  $h(x_{u2}) > h_2$  and because no undulations are present El et al. (2006) results are not applicable to these solutions.

Convergence is also present in Figure 5 with both the  $L_1$  and  $C_1$  measures. Here  $L_1$  has been modified to use the numerical solution when  $\Delta x = 10/2^{10} m$  as an approximation to the analytic solution because none are currently known for the Serre equations. For  $L_1$  and  $C_1$  of  $\mathcal{H}$  the order of accuracy is the theoretical one. Since  $L_1$  compares only numerical results, round-off errors result in error stagnation rather than increase as in Figure ???.  $C_1$  for  $h$  demonstrates that the finite volume method does indeed conserve mass independent of  $\Delta x$  with round-off errors dominant for all tested  $\Delta x$ .  $C_1$  of  $uh$  has been omitted because there is a small but noticeable flux of momentum at the boundaries due to the large  $\alpha$ , which dominates the errors and cannot be accounted for. The presented measures suggest that this family of solutions is an accurate representation of the behaviour of the Serre equations when  $\alpha$  is sufficiently large and in particular  $\alpha = 40m$ .

The second behaviour will be referred to as the flat behaviour due to the presence of a constant height around  $x_{u2}$ , this is the most common behaviour observed in the literature (Le Métayer et al. 2010; Mitsotakis et al. 2014; Mitsotakis et al. 2016). This behaviour has oscillations in regions III and IV which are separated by a constant height state around  $x_{u2}$ . An example of the numerical results for this behaviour can be seen in Figure 6 when  $\alpha = 2m$ .

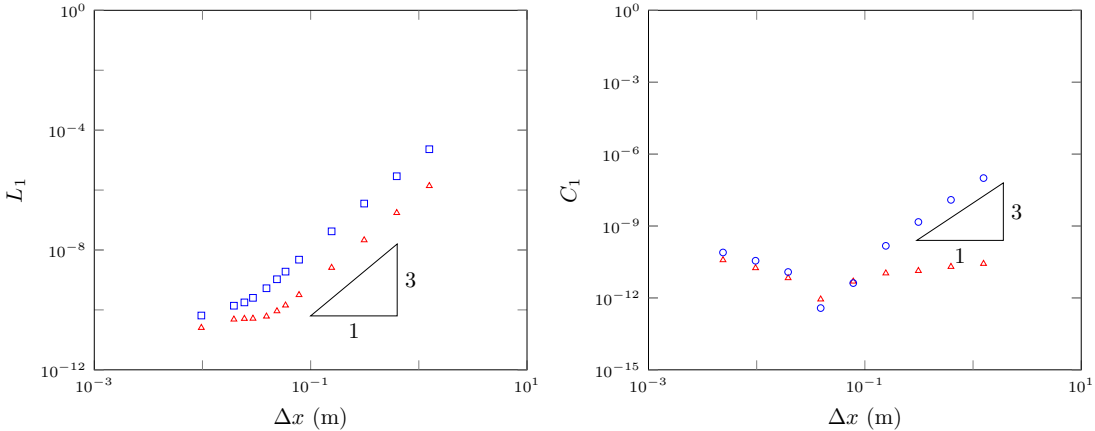


FIG. 5: On the left is  $L_1$  for  $h$  ( $\Delta$ ) and  $u$  ( $\square$ ) and on the right is  $C_1$  for  $h$  ( $\Delta$ ) and  $H$  ( $\circ$ ) for  $\mathcal{V}_3$ 's solution for the smooth dam-break problem with  $\alpha = 40m$ .

As  $\Delta x$  decreases the solutions converge so that by  $\Delta x = 10/2^8m$  the solutions for higher  $\Delta x$  are visually identical. There is also good agreement between the peak amplitude in region IV ( $A$ ) and  $A^+$  as well as  $h(x_{u_2})$  and  $h_2$ . Although as  $\Delta x$  is decreased in the simulations we observe  $h(x_{u_2}) > h_2$ . Since this method is well validated for smooth problems and a small  $\Delta x$  has been chosen this suggests that the mean bore heights in regions III and IV from a dam-break may differ slightly between the shallow water wave equations and the Serre equations. These results also compare well to the results in Mitsotakis et al. (2016) who use the same  $\alpha$  but different  $h_0$  and  $h_1$ . We observed this behaviour for  $\mathcal{V}_1$ 's simulations.

The measures  $L_1$  and  $C_1$  demonstrate good convergence with the expected order of accuracy. For  $\mathcal{V}_3$  we observe that  $C_1$  of  $uh$  has a larger error but a higher order of accuracy than  $C_1$  of  $H$ . The higher order of accuracy makes sense as the conversion between the conserved quantity  $G$  and  $u$  is fourth order. The smaller  $C_1$  error of  $H$  can be explained by noting that although  $uh$  is a component of  $H$ ,  $gh^2$  makes up a far larger portion of  $H$  see Figure 19, diminishing the relative size of the  $uh$  errors in  $H$ .

These results demonstrate that this behaviour is an accurate representation of the nature of the Serre equations provided  $\alpha$  is large enough supporting the findings of Mitsotakis et al. (2016).

The third behaviour will be referred to as the node behaviour and it was observed by El et al. (2006). The node behaviour's main feature is that the oscillations in region III and IV decay and appear to meet at  $x_{u_2}$  as can be seen in Figure 8 when  $\alpha = 0.4m$ . All the methods have not converged to a solution as  $\Delta x$  decreases. However, it does appear that convergence is likely with the solutions getting closer together. This is expected for the smaller  $\Delta x$  because the problem is still smooth. In these results  $A^+$  is a good estimator for  $A$  and the oscillations in regions III and IV appear to be around  $h_2$ . This behaviour was observed by El et al. (2006) for  $\mathcal{E}$  and indeed we have replicated it for all the high order methods. It was not observed in  $\mathcal{V}_1$ 's solutions up to  $\Delta x = 10/2^{10}m$  with  $\alpha = 0.001m$  as  $\mathcal{V}_1$  introduces diffusive errors that severely

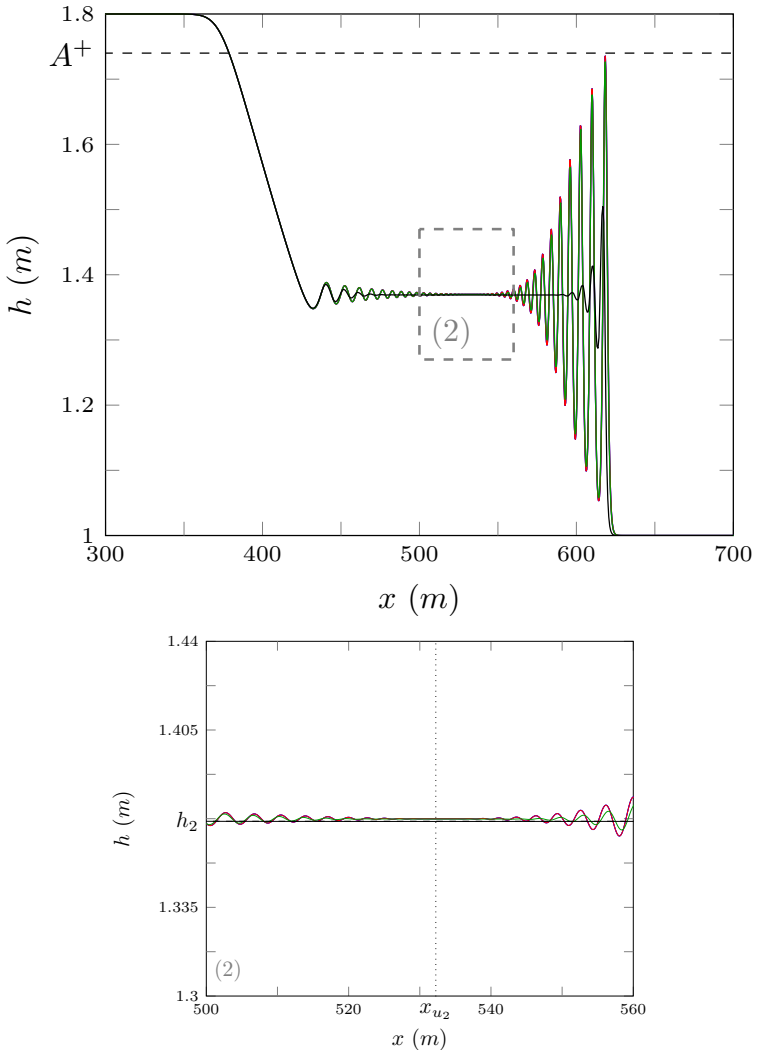


FIG. 6: Numerical results of  $\mathcal{V}_3$  at  $t = 30s$  for the smooth dam-break problem with  $\alpha = 2m$  for  $\Delta x = 10/2^{10}m$  (—),  $10/2^8m$  (—),  $10/2^6m$  (—) and  $10/2^4m$  (—).

222 dampen the oscillations. This explains why Le Métayer et al. (2010) using  $\mathcal{V}_1$  could  
 223 not replicate the results of El et al. (2006). It was found that an  $\alpha$  of at least  $0.4m$  is  
 224 required to recover the node behaviour this explains why Mitsotakis et al. (2016) and  
 225 Mitsotakis et al. (2014) using  $\alpha$ 's of  $2m$  and  $1m$  respectively could not replicate the  
 226 results of El et al. (2006).

227 The assertion that these results are close to converging to a solution is supported  
 228 by Figure 9 with appropriate orders of accuracy for  $L_1^*$  and  $C_1$ . Figure 8 demon-  
 229 strates that the final solutions have not yet converged, thus we modify  $L_1$  to omit  
 230  $[520m, 540m]$  and call this modified measure  $L_1^*$ .  $L_1^*$  demonstrates that even though  
 231 the section around  $x_{u_2}$  has not been fully resolved we do see that there is convergence  
 232 at the appropriate order away from  $x_{u_2}$ . This suggests that the effect of better resolv-  
 233 ing the oscillations will only be felt locally.  $C_1$  demonstrates the appropriate order of

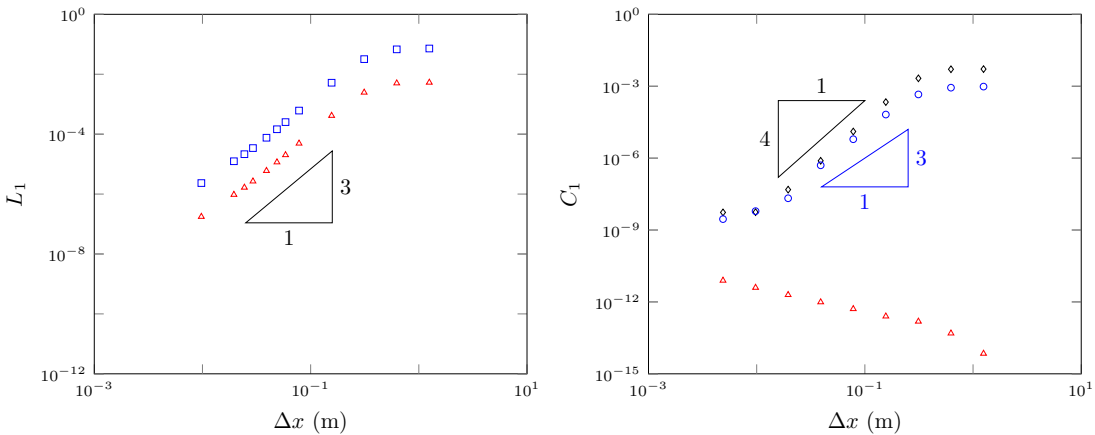


FIG. 7: On the left is  $L_1$  for  $h$  ( $\triangle$ ) and  $u$  ( $\square$ ) and on the right is  $C_1$  for  $h$  ( $\triangle$ ),  $uh$  ( $\diamond$ ) and  $\mathcal{H}$  ( $\circ$ ) for  $\mathcal{V}_3$ 's solution for the smooth dam-break problem with  $\alpha = 2m$ .

accuracy in conserving momentum and the Hamiltonian suggesting that we are indeed approaching a reasonable solution to this problem as  $\Delta x$  is decreased.

These results demonstrate that although we have not yet fully converged this behaviour is close to reasonable solutions of the Serre equations given the appropriate  $\alpha$  value supporting the findings of El et al. (2006).

The fourth behaviour will be referred to as the bump behaviour due to the oscillations no longer decaying down towards a point but rather growing around  $x_{u_2}$  forming a bump as can be seen in Figure 10 for  $\alpha = 0.1m$ . This behaviour has hitherto not been published and is certainly not an expected result.

This behaviour is even further from converging with decreasing  $\Delta x$  around  $x_{u_2}$  than the node behaviour as can be seen in Figure 10.  $L_1^*$  demonstrates good convergence outside this middle region as can be seen in Figure 11 so that resolving the region around  $x_{u_2}$  is the main difficulty for our numerical methods.  $C_1$  of  $uh$  and  $\mathcal{H}$  also converges but compared to the other behaviours we have lost an order of accuracy in these measures. This suggests that we are not using the appropriate  $\Delta x$  and thus smaller grids are required to attain the appropriate order of convergence for  $\mathcal{V}_3$ . Because, convergence is not assured by these numerical results there is the possibility that the wave amplitudes around the  $x_{u_2}$  could grow rapidly. This however has not been observed, with numerical results where  $\alpha = 0.001m$  and  $\Delta x = 10.0/2^{10}m$  at which point the initial conditions are basically a discontinuous dam-break showing an increase but not a large growth in the amplitude of the bump for  $\mathcal{V}_3$ .

Since this result is unexpected and not as supported as the node behaviour in the literature (El et al. 2006). The first check should be different numerical methods such as  $\mathcal{G}$  and  $\mathcal{E}$  to test if some numerical effect from the reformulation of the Serre equations or the elliptic solver are the cause. For comparison  $\mathcal{G}$ ,  $\mathcal{E}$ ,  $\mathcal{V}_1$  and  $\mathcal{V}_3$  are applied to the same initial conditions with the same grid resolutions as above and the results were plotted in Figure 12.  $\mathcal{V}_2$  has been omitted from this figure for clarity because its solution is very close to  $\mathcal{V}_3$  as noted by Zoppou et al. (2017). The first observation is that

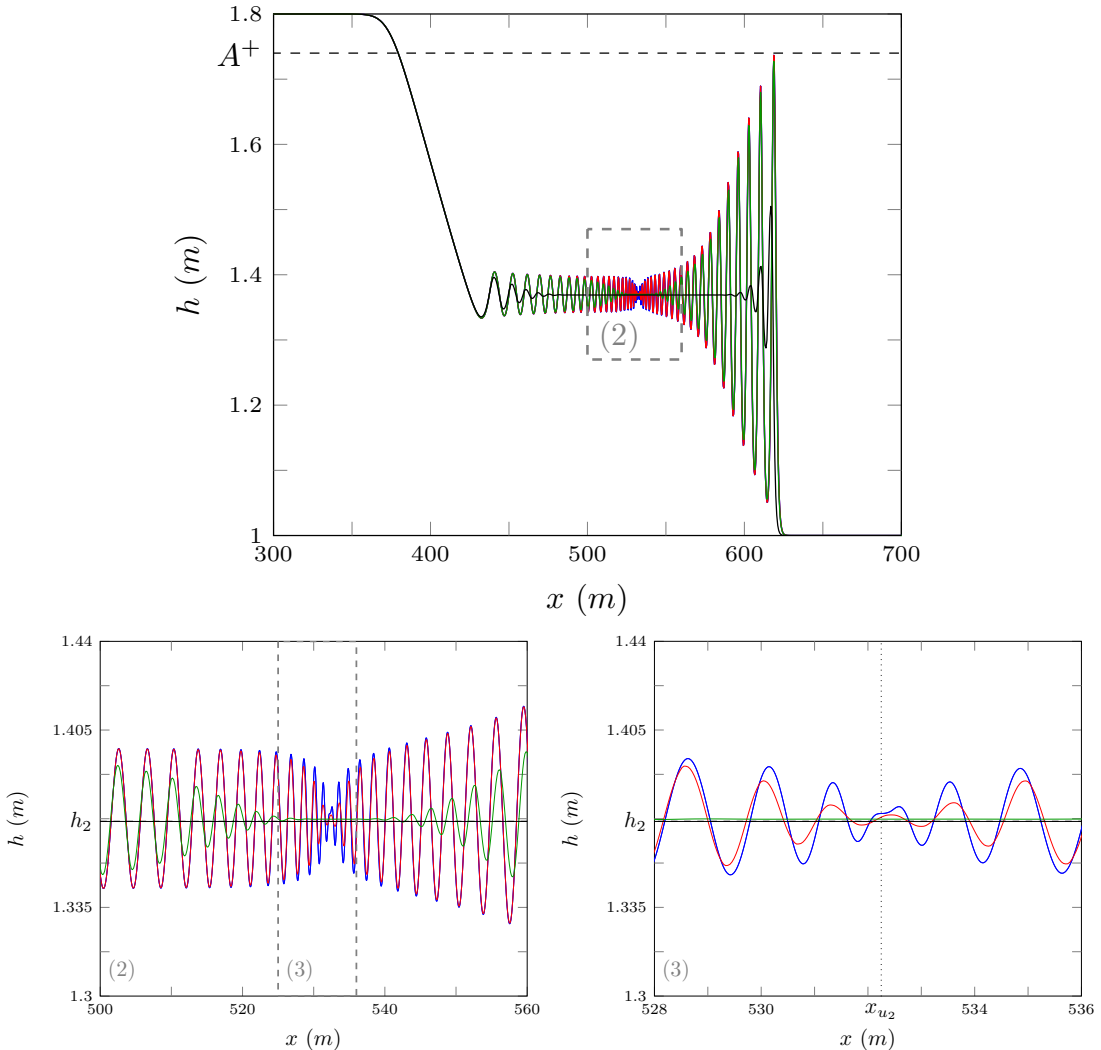


FIG. 8: Numerical results of  $\mathcal{V}_3$  at  $t = 30s$  for the smooth dam-break problem with  $\alpha = 0.4m$  for  $\Delta x = 10/2^{10}m$  (—),  $10/2^8m$  (—),  $10/2^6m$  (—) and  $10/2^4m$  (—).

$\mathcal{V}_1$  has not recovered this behaviour. This is because  $\mathcal{V}_1$  is very diffusive (Zoppou et al. 2017), dampening these oscillations. To resolve such behaviour for  $\mathcal{V}_1$  would require very small  $\Delta x$  and as such this has not been observed in the simulations. Secondly, all high-order methods recover this bump behaviour and disagree only in the region around  $x_{u_2}$ . The main difference in the oscillations is their phase and amplitude with the dispersive finite difference methods resulting in larger waves than the diffusive finite difference-volume hybrid methods. We also observe oscillations in  $\mathcal{E}$  that are not replicated by the other methods close to  $x_{u_2}$ , this is caused by the instability of  $\mathcal{E}$  with its effects being more obvious here due to the high frequency of these waves which correspond to larger growth factors.

Since  $\mathcal{V}_3$  is diffusive as can be seen in Figure 10 and  $\mathcal{G}$  is dispersive the true analytic solution should exist between  $\mathcal{V}_3$  and  $\mathcal{G}$ , which is a bounded bump around  $x_{u_2}$ .  $\mathcal{G}$  well

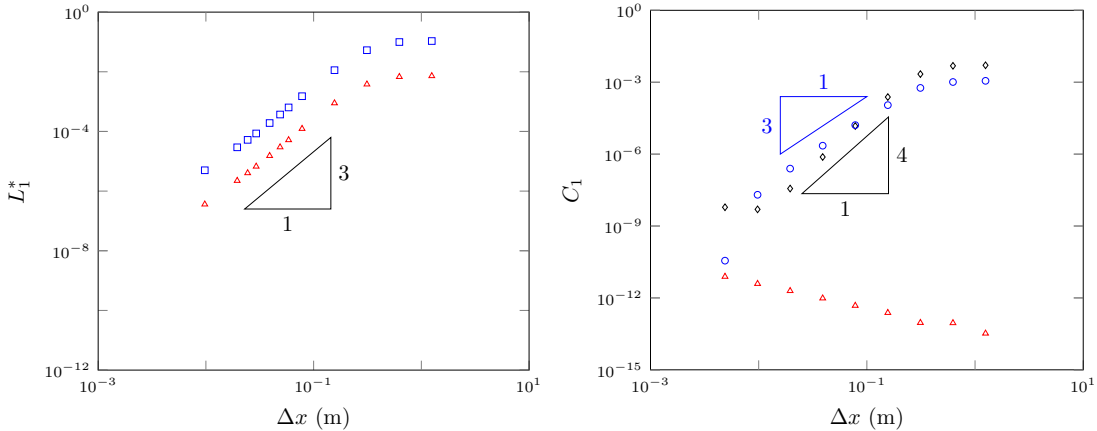


FIG. 9: On the left is  $L_1^*$  for  $h$  ( $\Delta$ ) and  $u$  ( $\square$ ) and on the right is  $C_1$  for  $h$  ( $\Delta$ ),  $uh$  ( $\diamond$ ) and  $H$  ( $\circ$ ) for  $\mathcal{V}_3$ 's solution for the smooth dam-break problem with  $\alpha = 0.4m$ .

274 approximates the Serre equations, although  $\mathcal{V}_2$  and  $\mathcal{V}_3$  are still preferred by the authors  
275 due to their robustness and superior conservation of quantities.

276 There is still the possibility that these solutions are caused by some numerical phe-  
277 nomena, more research into this topic should be undertaken. However, the agreement  
278 of all the discussed methods of sufficiently high order indicates that these results are  
279 representative of actual solutions of the smoothed dam-break problem with low  $\alpha$  for  
280 the Serre equations. Lastly the bump behaviour was observed using  $\mathcal{E}$  with a similar  
281 order of magnitude for  $\Delta x$  and  $\Delta t$  as El et al. (2006). The absence of a bump be-  
282 haviour in their findings is caused by the smoothing of the initial conditions which is  
283 absent from the paper but was confirmed later by El and Hoefer (2016).

284 This concludes the explanation of how our results fit in with the current literature  
285 and the following section of this paper will be concerned with some further numerical  
286 investigation into these results.

#### 287 *Long time*

288 The first test of these results will be of its evolution through time, thus an experi-  
289 ment was run with the same parameters on a larger domain with  $x \in [-900m, 1800m]$   
290 for  $t \in [0, 300s]$ . The results of  $\mathcal{V}_3$  with  $\alpha = 0.1m$  and  $\Delta x = 10/2^9m$  and  $10/2^8m$  at  
291  $t = 300s$  are presented in Figure 13. For this problem these parameters result in the  
292 bump behaviour as can be seen in Figure 10, however after sufficient time we can see  
293 that this bump behaviour has decayed back into a flat behaviour although there are still  
294 small oscillations present in the middle region.

295 We also observe that  $A^+$  has not been perfectly replicated with the numerical so-  
296 lution having larger peak amplitudes in region IV than  $A^+$ . Consequently we can see  
297 that while  $x_{S^+}$  is a better approximation than  $x_{S_2}$  to the position of the bore it is still  
298 an underestimate. Thus our bores will arrive a little earlier than predicted by  $S^+$  and  
299 much earlier than predicted by  $S_2$ . We also note that as above the bore heights for the  
300 Serre and shallow water wave equations appear to be slightly different.

301 To track the decaying of the oscillations for  $\mathcal{V}_3$ 's solution around  $x_{u_2}$  a snapshot of

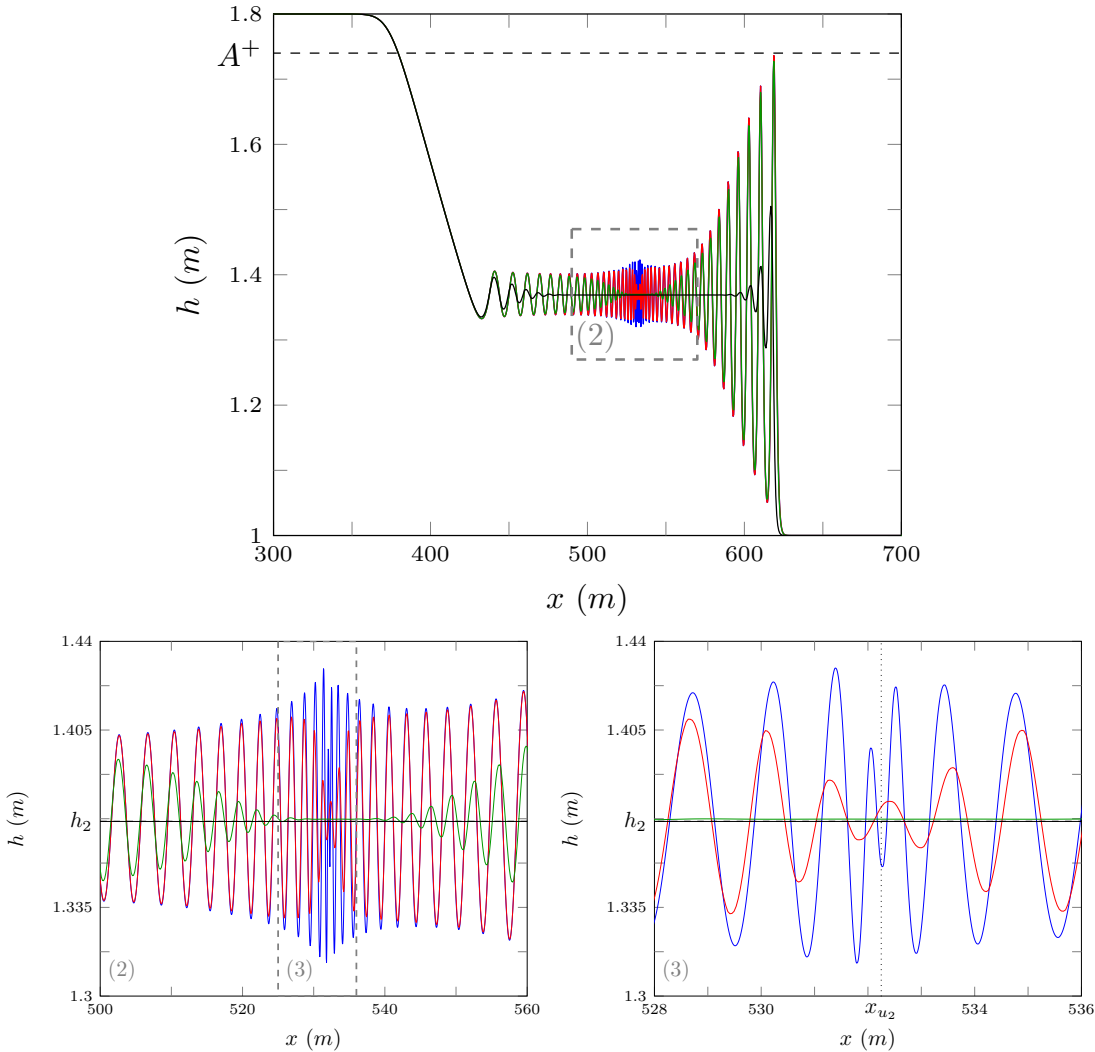


FIG. 10: Numerical results of  $\mathcal{V}_3$  at  $t = 30s$  for the smooth dam-break problem with  $\alpha = 0.1m$  for  $\Delta x = 10/2^{10}m$  (—),  $10/2^8m$  (—),  $10/2^6m$  (—) and  $10/2^4m$  (—).

302 the area around  $x_{u2}$  has been plotted for different times in Figure 14. It can be seen that  
 303 at  $t = 30s$  the solution exhibits the bump behaviour but as time progresses the region  
 304 around  $x_{u2}$  has decayed into the node behaviour by  $t = 100s$  and then into the flat  
 305 behaviour observed at  $t = 200s$  and  $t = 300s$ . This could be a property of the solution  
 306 of the Serre equations after sufficient time or due to the accumulation of diffusive errors  
 307 of the numerical method with Figure 13 demonstrating that over this time span we are  
 308 not close to convergence of the numerical results. We note that El et al. (2006) had  
 309 very similar results in this longer time scale although their paper uses the normalised  
 310 Serre equations so that in effect  $g = 1m/s^2$  and an unknown smoothing of the initial  
 311 conditions which make comparisons of the solutions at similar times difficult.

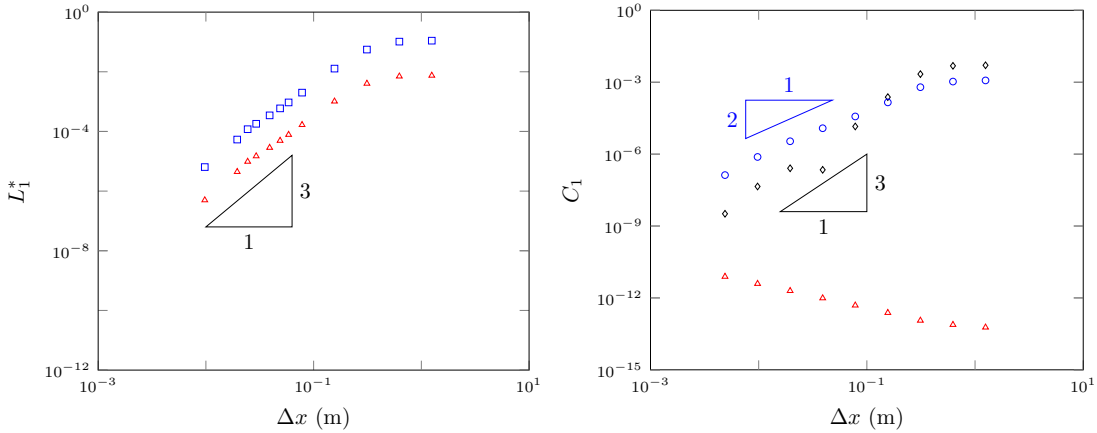


FIG. 11: On the left is  $L_1^*$  for  $h$  ( $\triangle$ ) and  $u$  ( $\square$ ) and on the right is  $C_1$  for  $h$  ( $\triangle$ ),  $uh$  ( $\diamond$ ) and  $H$  ( $\circ$ ) for  $\mathcal{V}_3$ 's solution for the smooth dam-break problem with  $\alpha = 0.1m$ .

312 *Shallow water wave equation comparison*

313 Since the shallow water wave equations have been used as a guide for the mean  
 314 behaviour of the solution of the Serre equations in the literature (Le Métayer et al.  
 315 2010; Mitsotakis et al. 2016) we would like to investigate how useful they are. We  
 316 first plot  $h - h_2$  and  $u - u_2$  for the smoothed dam-break problem with  $\alpha = 0.1m$  and  
 317  $\Delta x = 10/2^9 m$  in Figure 15 for  $t = 30s$  and Figure 16 for  $t = 300s$ . From this we  
 318 can see that over short time spans both  $h_2$  and  $u_2$  are good approximations to the mean  
 319 behaviour of the fluid with both plots oscillating around 0. However after sufficient  
 320 time we see that the mean velocity and height of the fluid have diverged slightly from  
 321 the shallow water wave equation values  $h_2$  and  $u_2$ . With  $h_2$  being an underestimate and  
 322  $u_2$  being an overestimate. From Figure 13 it can also be seen that  $S_2$  underestimates  
 323 the speed of the bore front.

324 From Figure 15 and Figure 16 it can be seen that to the left of  $x_{u_2}$   $u$  and  $h$  are  
 325 anti-phase while to the right of  $x_{u_2}$   $u$  and  $h$  are in-phase. The contact discontinuity  
 326 (El et al. 2006) marks the transition between these two states which is located at about  
 327  $x_{u_2}$ . Figure 16 demonstrates that at  $x_{u_2}$ ,  $h$  and  $u$  are in-phase therefore the contact  
 328 discontinuity is to the left of  $x_{u_2}$ , thus the speed of the contact discontinuity like the  
 329 mean bore velocity is slightly overestimated by  $u_2$ .

330 Because  $h$  and  $u$  are anti-phase to the left of the contact discontinuity they appear to  
 331 travel leftwards relative to it while those on the right are in-phase and therefore appear  
 332 to travel rightwards relative to the contact discontinuity. Thus these oscillations appear  
 333 to be forming at the contact discontinuity and then travelling away from it. The phase  
 334 velocity of the linearised Serre equations is

$$v_p = u \pm \sqrt{gh} \sqrt{\frac{3}{h^2 k^2 + 3}}$$

335 where  $k$  is the wave number. The phase velocity has the following behaviour, as  $k \rightarrow$   
 336  $\infty$  then  $v_p \rightarrow u$  and as  $k \rightarrow 0$  then  $v_p \rightarrow u \pm \sqrt{gh}$ . Since we observe  $u$  and  $h$

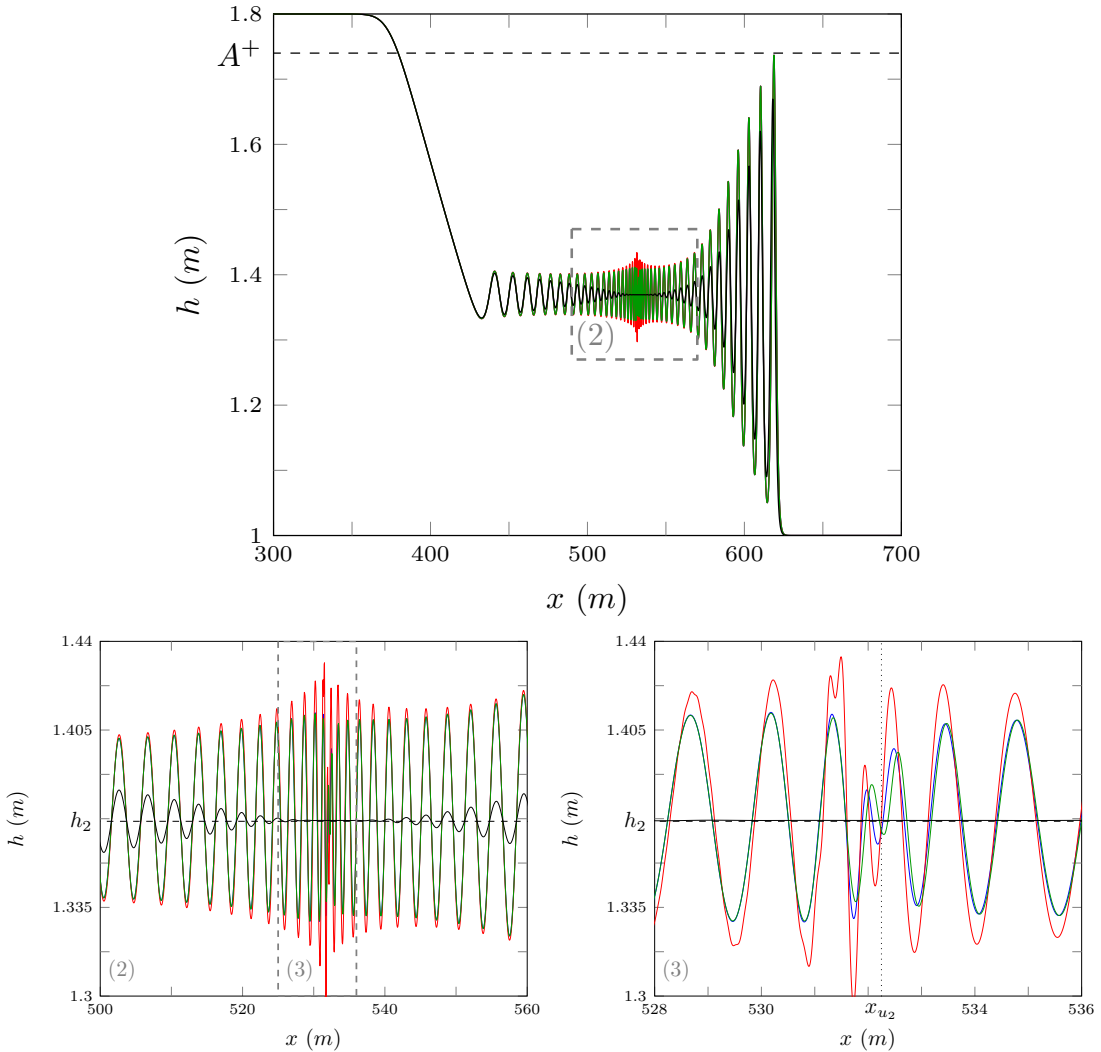


FIG. 12: Numerical results for the smooth dam-break problem with  $\alpha = 0.1m$  and  $\Delta x = 10/2^{10}m$  for  $\mathcal{G}$  (—),  $\mathcal{E}$  (—),  $\mathcal{V}_3$  (—) and  $\mathcal{V}_1$  (—).

as being anti-phase to the left of the contact discontinuity this means we are in the negative branch of the phase velocity  $u - \sqrt{gh}\sqrt{\frac{3}{h^2k^2+3}}$  while the in-phase right side corresponds to the positive branch  $u + \sqrt{gh}\sqrt{\frac{3}{h^2k^2+3}}$ . Thus the contact discontinuity corresponds to oscillations with very high wave numbers, which are sensitive to both smoothing of the initial conditions and numerical diffusion. By this phase velocity argument the contact discontinuity should travel at the mean bore velocity which is close to  $u_2$  for a range of dam-break problems. To investigate this  $h_0 = 1m$  was fixed and  $h_1$  was varied to allow for different aspect ratios and thus different bore speeds. The results are plotted in Figure 17 from which it is quite clear that the contact discontinuity does in fact travel at close to  $u_2$  for a range of aspect ratios.

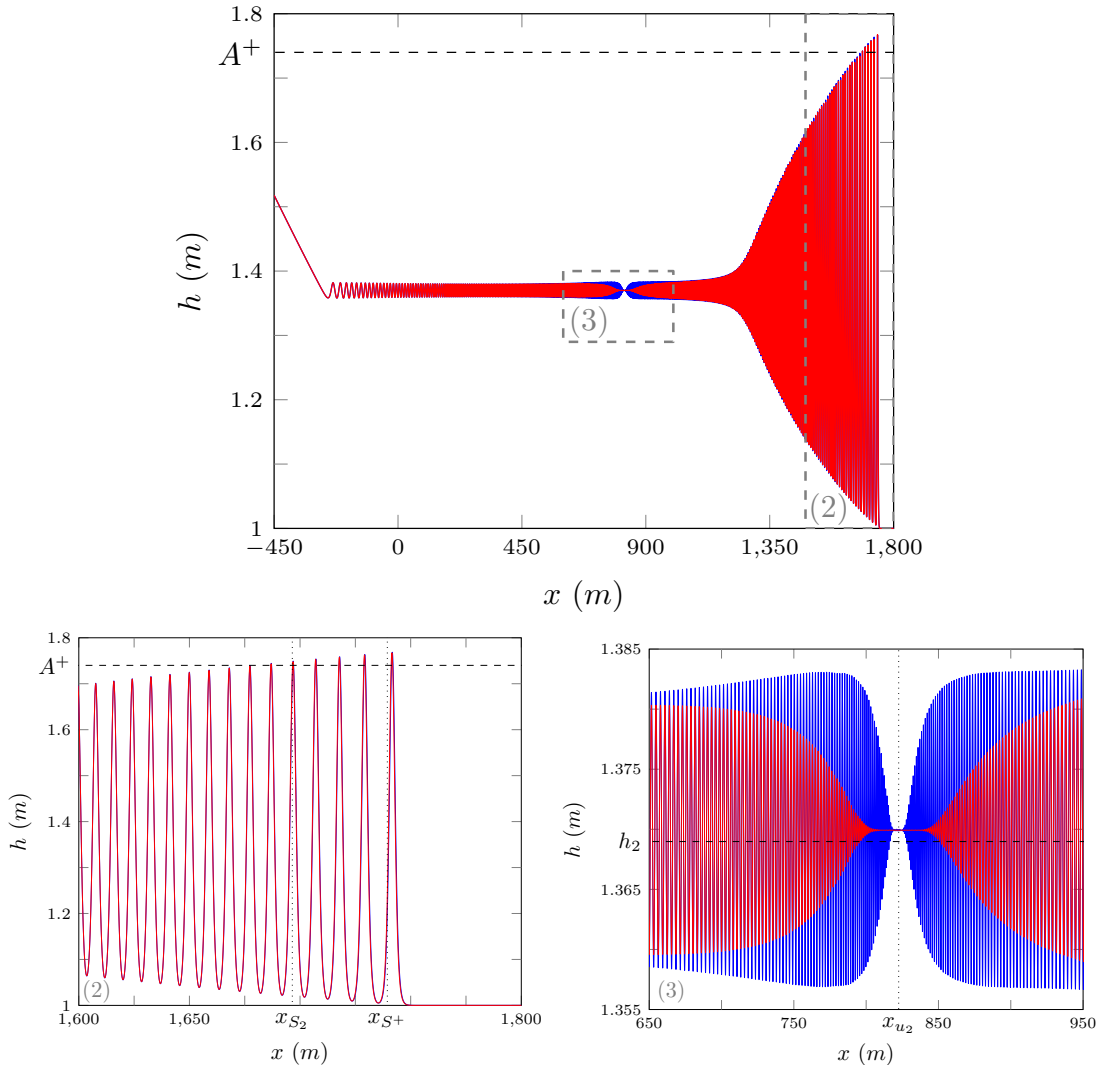


FIG. 13: Numerical solution of smooth dam-break problem at  $t = 300s$  by  $\mathcal{V}_3$  with  $\alpha = 0.1m$  for  $\Delta x = 10/2^9 m$  (—) and  $10/2^8 m$  (—).

347    *Whitham modulation comparison*

348    The expressions for the leading wave amplitude  $A^+$  and speed  $S^+$  obtained by  
 349    El et al. (2006) are asymptotic results and so we are interested in how our numerical  
 350    results behave over time. Thus for the dam-break problem in Figure 13 the peak am-  
 351    plitude in region IV ( $A$ ) was plotted over time in Figure 18. From the figure it can see  
 352    that  $A$  approaches a value larger than  $A^+$ . We find that as  $\alpha \rightarrow 0$  and  $\Delta x \rightarrow 0$  our  
 353     $A$  values converge away from  $A^+$  not towards it in this time scale for this aspect ratio.  
 354    Thus it appears that the true solution of the dam-break for the Serre equations has an  
 355    amplitude in region IV slightly above  $A^+$ . This is not inconsistent with the results of  
 356    (El et al. 2006) as their scale comparing  $A^+$  to numerical solutions is too large to see  
 357    such a small difference. From Figure 13 it can be seen that while  $S^+$  does not precisely  
 358    predict the bore speed it is a better prediction than  $S_2$ .

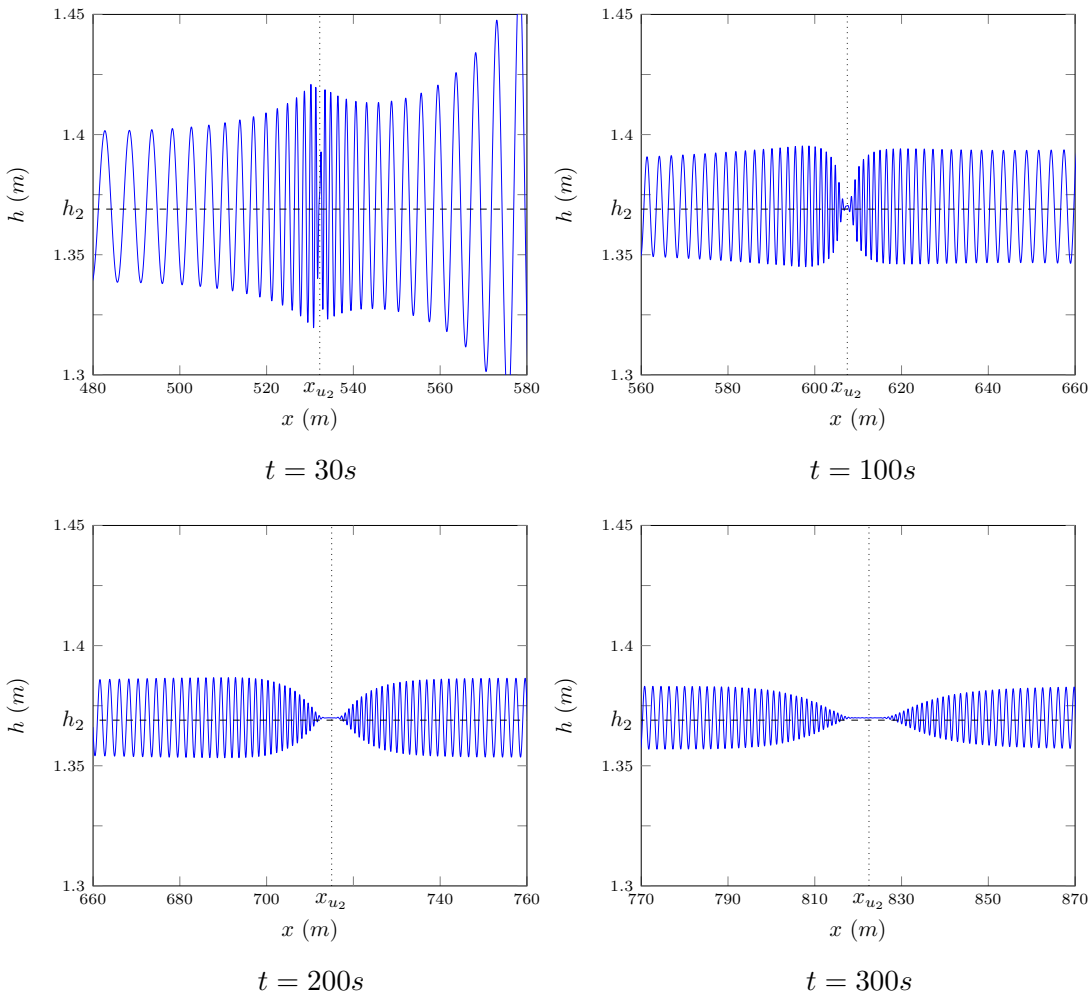


FIG. 14: Numerical solution of the smooth dam-break problem by  $\mathcal{V}_3$  with  $\alpha = 0.1m$  and  $\Delta x = 10/2^9 m$  at various times.

359 *Energy Breakdown*

360 The Hamiltonian (2) has 3 terms representing in order, horizontal kinetic energy  
 361  $hu^2$ , vertical kinetic energy  $\frac{h^3}{3} \frac{\partial u}{\partial x}$  and gravitational potential energy  $gh^2$ . It might be  
 362 expected that the oscillations of the undular bore such as in Figure 13 would result in  
 363 significant vertical energies. However, Figure 19 demonstrates that this is not the case,  
 364 as the total vertical kinetic energy in the system is insignificant relative to the other  
 365 energies. This plot also demonstrates that even with dispersive terms and large oscil-  
 366 lations the drivers of change in the dam-break problem are the transfer of gravitational  
 367 potential energy into horizontal kinetic energy which occurs slowly.

368 **CONCLUSIONS**

369 Utilising two finite difference methods of second-order and three finite difference-  
 370 volume hybrid methods of various orders an investigation into the smoothed dam-break  
 371 problem with varying steepness was performed. Four different behaviours were uncov-

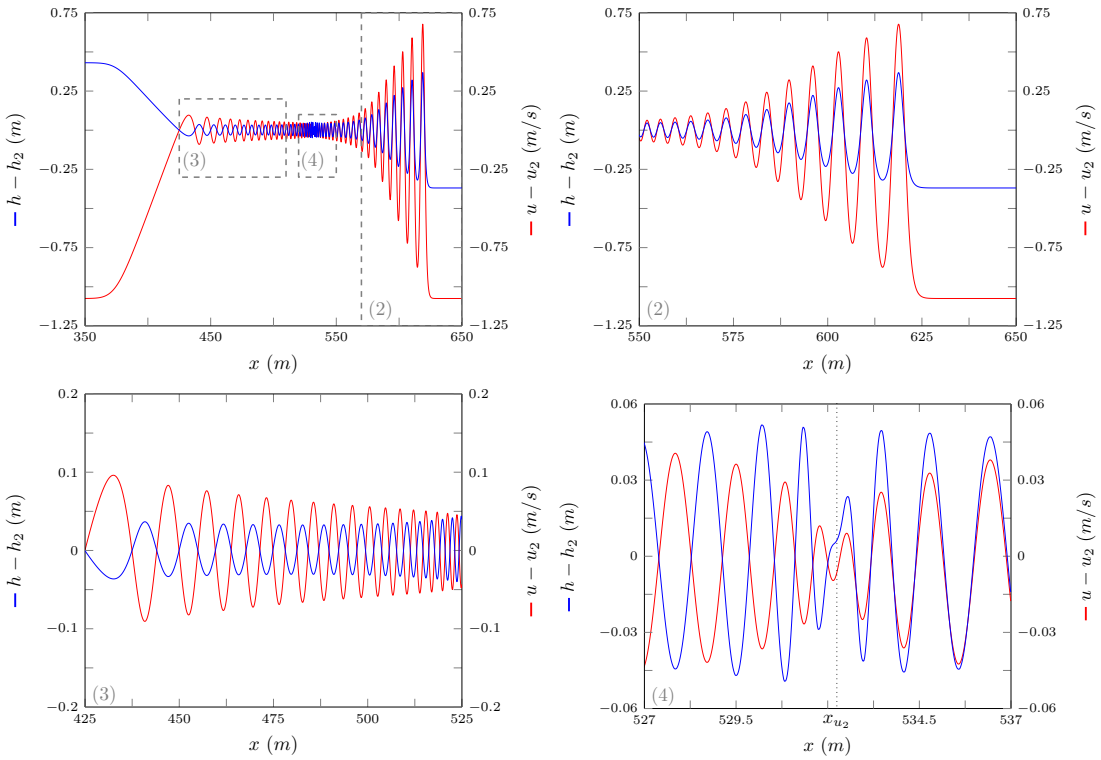


FIG. 15:  $h - h_2$  (—) and  $u - u_2$  (—) for numerical solution of the smooth dam-break by  $\mathcal{V}_3$  with  $\alpha = 0.1m$  and  $\Delta x = 10/2^9 m$  at  $t = 30s$  as in Figure 10.

372 ered with the general trend being that an increase in steepness increases the size and  
 373 number of oscillations in the solution. This study explains all current differences in the  
 374 literature involving the solution of the Serre equations applied to the smoothed dam-  
 375 break problem and also uncovers a new result. We find that while the analytic solution  
 376 of the shallow water wave equations for the dam-break problem is a good guide to the  
 377 mean behaviour of the Serre equations the speed and height of the bores do not match  
 378 up precisely. While the Whitham modulation results for the Serre equations give bet-  
 379 ter predictions than the shallow water wave equations analytic solution it was found  
 380 that they also do not line up with our numerical results precisely. It was demonstrated  
 381 that the contact discontinuity corresponds to high wave numbers and thus travels at  
 382 the mean velocity inside the bore. It was also found that vertical kinetic energy is  
 383 negligible for the dam-break problem.

## 384 REFERENCES

- 385 A. Harten, A. (1983). “High resolution schemes for hyperbolic conservation laws.”  
 386 *Journal of Computational Physics*, 49(3), 357–393.  
 387 Carter, J. D. and Cienfuegos, R. (2011). “Solitary and cnoidal wave solutions of the  
 388 Serre equations and their stability.” *European Journal of Mechanics B/Fluids*, 30(3),  
 389 259–268.  
 390 El, G., Grimshaw, R. H. J., and Smyth, N. F. (2006). “Unsteady undular bores in fully  
 391 nonlinear shallow-water theory.” *Physics of Fluids*, 18(027104).

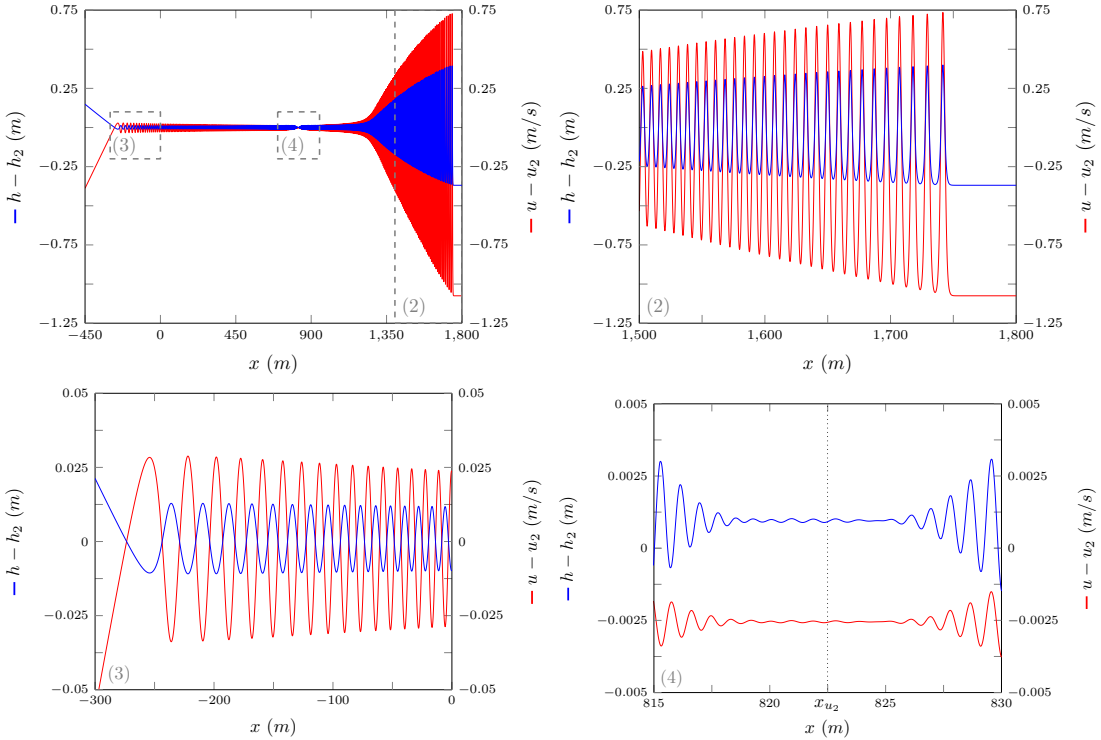


FIG. 16:  $h - h_2$  (—) and  $u - u_2$  (—) for numerical solution of the smooth dam-break by  $\mathcal{V}_3$  with  $\alpha = 0.1m$  and  $\Delta x = 10/2^9 m$  at  $t = 300s$  as in Figure 13.

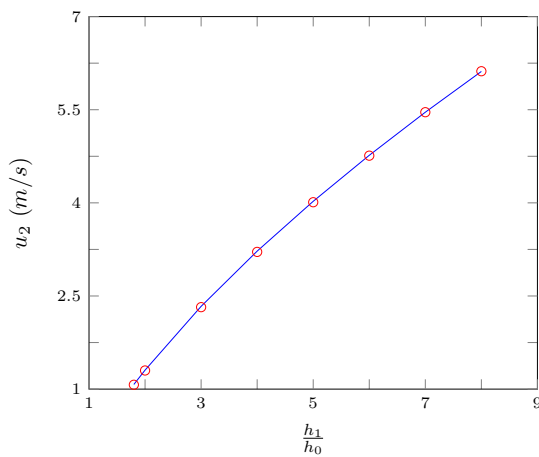


FIG. 17:  $u_2$  (—) and speed of the contact discontinuity (○) for numerical solutions of smoothed dam-break problems with different aspect ratios ( $h_1/h_0$ ) by  $\mathcal{V}_3$  where  $\alpha = 0.1m$  and  $\Delta x = 10/2^9 m$  at  $t = 100s$ .

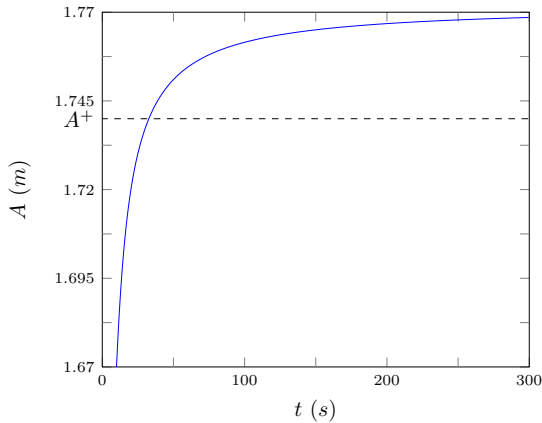


FIG. 18: Leading wave height plotted over time for the numerical solution of the smooth dam-break problem by  $\mathcal{V}_3$  with  $\alpha = 0.1m$  for  $\Delta x = 10/2^9m$  (—) as in Figure 13.

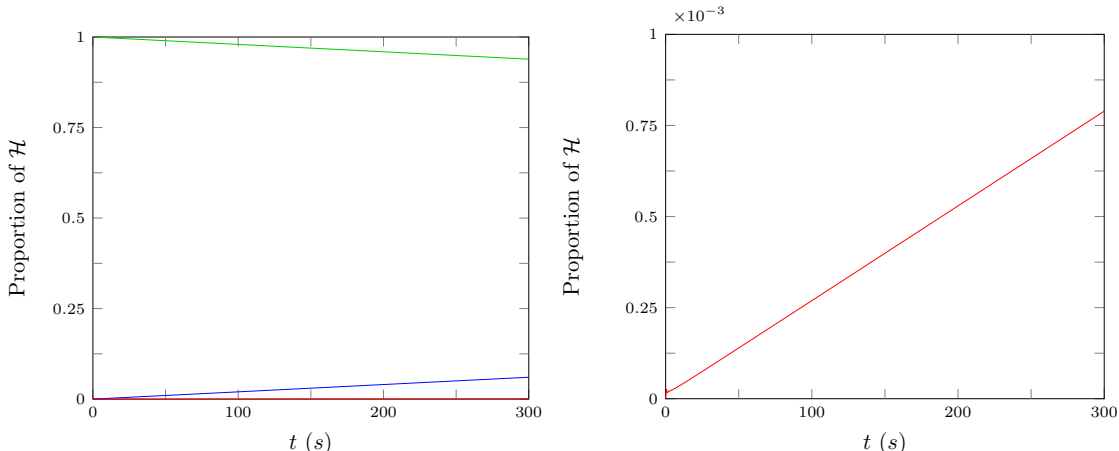


FIG. 19: Proportion of  $\mathcal{H}$  made up by horizontal kinetic energy (—), vertical kinetic energy (—) and gravitational potential energy (—) for  $\mathcal{V}_3$ 's solution of the smooth dam-break problem with  $\alpha = 0.1m$  and  $\Delta x = 10/2^9m$  over time as in Figure 13.

- 392 El, G. and Hoefer, M. (2016). “Dispersive shock waves and modulation theory.” *Phys-  
393 ica D: Nonlinear Phenomena*, 333, 11–65.  
394 Green, A. E. and Naghdi, P. M. (1976). “A derivation of equations for wave propagation  
395 in water of variable depth.” *Journal of Fluid Mechanics*, 78(2), 237–246.  
396 Lannes, D. and Bonneton, P. (2009).” *Physics of Fluids*, 21(1), 16601–16610.  
397 Le Métayer, O., Gavrilov, S., and Hank, S. (2010). “A numerical scheme for the  
398 GreenNaghdi model.” *Journal of Computational Physics*, 229(6), 2034–2045.  
399 Li, M., Guyenne, P., Li, F., and Xu, L. (2014). “High order well-balanced CDG-FE  
400 methods for shallow water waves by a Green-Naghdi model.” *Journal of Compu-  
401 tational Physics*, 257, 169–192.  
402 Li, Y. A. (2002). “Hamiltonian Structure and Linear Stability of Solitary Waves of the

- 403 Green-Naghdi Equations." *Journal of Nonlinear Mathematical Physics*, 9, 99–105.  
 404 Mitsotakis, D., Dutykh, D., and Carter, J. (2016). "On the nonlinear dynamics of the  
 405 traveling-wave solutions of the serre system." *Wave Motion*.  
 406 Mitsotakis, D., Ilan, B., and Dutykh, D. (2014). "On the Galerkin/Finite-Element  
 407 Method for the Serre Equations." *Journal of Scientific Computing*, 61(1), 166–195.  
 408 Su, C. H. and Gardner, C. S. (1969). "Korteweg-de Vries equation and generalisations.  
 409 III. Derivation of the Korteweg-de Vries equation and Burgers equation." *Journal of  
 410 Mathematical Physics*, 10(3), 536–539.  
 411 Wu, C., Huang, G., and Zheng, Y. (1999). "Theoretical solution of dam-break shock  
 412 wave." *Journal of Hydraulic Engineering*, 125(11), 1210–1215.  
 413 Zoppou, C. (2014). "Numerical solution of the One-dimensional and Cylindrical Serre  
 414 Equations for Rapidly Varying Free Surface Flows." Ph.D. thesis, Australian Na-  
 415 tional University, Mathematical Sciences Institute, College of Physical and Mathe-  
 416 matical Sciences, Australian National University, Canberra, ACT 2600, Australia.  
 417 Zoppou, C., Pitt, J., and Roberts, S. (2017). "Numerical solution of the fully non-linear  
 418 weakly dispersive serre equations for steep gradient flows." *Applied Mathematical  
 419 Modelling*, 00(00), 00–00.

420 **APPENDIX**

421 **Numerical Methods for Solving the Serre Equations**

422 *Second Order Centered Finite Difference Approximation for the Conservation of Mo-*  
 423 *mentum Equation*

424 The finite difference approximation to (1b) on a uniform grid in space such that  
 425  $\Delta x = x_{i+1} - x_i \forall i$  and a uniform grid in time such that  $\Delta t = t^{n+1} - t^n \forall n$  is

$$426 h_i^n u_i^{n+1} - (h_i^n)^2 \left( \frac{u_{i+1}^{n+1} - u_{i-1}^{n+1}}{2\Delta x} \right) - \frac{(h_i^n)^3}{3} \left( \frac{u_{i+1}^{n+1} - 2u_i^{n+1} + u_{i-1}^{n+1}}{\Delta x^2} \right) = -Y_i^n \quad (7)$$

428 and

$$429 Y_i^n = 2\Delta t X_i^n - h_i^n u_i^{n-1} + (h_i^n)^2 \left( \frac{u_{i+1}^{n-1} - u_{i-1}^{n-1}}{2\Delta x} \right) + \frac{(h_i^n)^3}{3} \left( \frac{u_{i+1}^{n-1} - 2u_i^{n-1} + u_{i-1}^{n-1}}{\Delta x^2} \right)$$

431 where  $q_i^n = q(x_i, t^n)$ . Equation (7) can be rearranged into an explicit update scheme  
 432 for  $u$  given its current and previous values, so that

$$433 \begin{bmatrix} u_0^{n+1} \\ \vdots \\ u_m^{n+1} \end{bmatrix} = A^{-1} \begin{bmatrix} -Y_0^n \\ \vdots \\ -Y_m^n \end{bmatrix} =: \mathcal{G}_u(\mathbf{u}^n, \mathbf{h}^n, \mathbf{u}^{n-1}, \Delta x, \Delta t) \quad (8)$$

435 where  $A$  is a tri-diagonal matrix.

436 A Lax-Wendroff Scheme for the Conservation of Mass Equation

437 The two step Lax-Wendroff update for  $h$  is

$$438 \quad h_{i+1/2}^{n+1/2} = \frac{1}{2} (h_i^n + h_{i+1}^n) - \frac{\Delta t}{2\Delta x} (u_{i+1}^n h_{i+1}^n - h_i^n u_i^n),$$

440

$$441 \quad h_{i-1/2}^{n+1/2} = \frac{1}{2} (h_i^n + h_{i-1}^n) - \frac{\Delta t}{2\Delta x} (u_i^n h_i^n - h_{i-1}^n u_{i-1}^n)$$

443 and

$$444 \quad h_i^{n+1} = h_i^n - \frac{\Delta t}{\Delta x} (u_{i+1/2}^{n+1/2} h_{i+1/2}^{n+1/2} - u_{i-1/2}^{n+1/2} h_{i-1/2}^{n+1/2}).$$

446 The quantities  $u_{i\pm 1/2}^{n+1/2}$  are calculated using  $u^{n+1}$  obtained by applying  $\mathcal{G}_u$  (8) to  $u^n$  then  
447 linearly interpolating in space and time to give

$$448 \quad u_{i+1/2}^{n+1/2} = \frac{u_{i+1}^{n+1} + u_{i+1}^n + u_i^{n+1} + u_i^n}{4}$$

450 and

$$451 \quad u_{i-1/2}^{n+1/2} = \frac{u_i^{n+1} + u_i^n + u_{i-1}^{n+1} + u_{i-1}^n}{4}.$$

453 Thus we have the following update scheme for (1a)

$$454 \quad \mathbf{h}^{n+1} = \mathcal{E}_h (\mathbf{u}^n, \mathbf{h}^n, \mathbf{u}^{n+1}, \Delta x, \Delta t). \quad (9)$$

456 Second-Order Centered Finite Difference Approximation for the Conservation of Mass  
457 Equation

458 The second order centered finite difference approximation to the conservation of  
459 mass equation (1a) is

$$460 \quad h_i^{n+1} = h_i^{n-1} - \Delta t \left( u_i^n \frac{h_{i+1}^n - h_{i-1}^n}{\Delta x} + h_i^n \frac{u_{i+1}^n - u_{i-1}^n}{\Delta x} \right).$$

462 Thus we have an update scheme for all  $i$

$$463 \quad \mathbf{h}^{n+1} = \mathcal{G}_h (\mathbf{u}^n, \mathbf{h}^n, \mathbf{h}^{n-1}, \Delta x, \Delta t). \quad (10)$$

465 Els Method for the Serre Equations

466 Els method (El et al. 2006) which we denote as  $\mathcal{E}$  is the combination of (9) for (1a)  
467 and (8) for (1b) in the following way

$$468 \quad \begin{aligned} \mathbf{u}^{n+1} &= \mathcal{G}_u (\mathbf{u}^n, \mathbf{h}^n, \mathbf{u}^{n-1}, \Delta x, \Delta t) \\ \mathbf{h}^{n+1} &= \mathcal{E}_h (\mathbf{u}^n, \mathbf{h}^n, \mathbf{u}^{n+1}, \Delta x, \Delta t) \end{aligned} \quad \left. \right\} \mathcal{E} (\mathbf{u}^n, \mathbf{h}^n, \mathbf{u}^{n-1}, \mathbf{h}^{n-1}, \Delta x, \Delta t). \quad (11)$$

470    *Second Order Centered Finite Difference Method for the Serre Equations*

471       The second order centered finite difference method for the Serre equations which  
472       we denote as  $\mathcal{G}$  is the combination of (10) for (1a) and (8) for (1b) in the following way

$$473 \quad \begin{aligned} \mathbf{h}^{n+1} &= \mathcal{G}_h(\mathbf{u}^n, \mathbf{h}^n, \mathbf{h}^{n-1}, \Delta x, \Delta t) \\ 474 \quad \mathbf{u}^{n+1} &= \mathcal{G}_u(\mathbf{u}^n, \mathbf{h}^n, \mathbf{u}^{n-1}, \Delta x, \Delta t) \end{aligned} \quad \left\} \mathcal{G}(\mathbf{u}^n, \mathbf{h}^n, \mathbf{u}^{n-1}, \mathbf{h}^{n-1}, \Delta x, \Delta t). \quad (12)$$

475    **Properties of Methods**

476    *Stability*

To ensure stability of the hybrid finite difference-volume methods the time-step  $\Delta t$  must satisfy the Courant-Friedrichs-Lowy (CFL) criteria (A. Harten 1983)

$$\Delta t < \frac{Cr\Delta x}{2 \max \{|\lambda|\}} \quad (13)$$

477       with  $0 < Cr \leq 1$  where  $\lambda$  is the characteristic speed. For the Serre equations it has  
478       been demonstrated that the wave speed is bounded by the characteristic speed of the  
479       shallow water wave equations (Le Métayer et al. 2010; Zoppou et al. 2017).

480       Performing a Von-Neumann stability analysis for  $\mathcal{G}$  (12) and  $\mathcal{E}$  (11) applied to  
481       the linearised Serre equations (Zoppou et al. 2017) it was found that the CFL condition  
482       (13) ensures stability for  $\mathcal{G}$ . It was also found that  $\mathcal{E}$  was stable with this CFL condition  
483       when there was no background flow. With some background flow  $\mathcal{E}$  is unconditionally  
484       unstable although we observed growth factors marginally above 1 for the flow regimes  
485       in this paper using the CFL condition, with smaller time-steps allowing for smaller  
486       growth factors.

487    *Convergence to Smooth Analytic Results*